

Binding of *Escherichia coli* to Functionalized Gold Nanoparticles

Pallavi Vedantam · Tzuen-Rong Jeremy Tzeng ·
Aaron Kenneth Brown · Ramakrishna Podila ·
Alekhya Rao · Kiesha Staley

Received: 4 August 2011 / Accepted: 20 November 2011 / Published online: 28 January 2012
© Springer Science+Business Media, LLC 2012

Abstract The molecular basis of the diversity of fimbrial lectins dictates the extent of adhesion in different types of *Escherichia coli* strains to mammalian cells. The mechanism of receptor binding by *E. coli* in eukaryotic cells differs based on the adhesin domains, patterns in the macromolecular structure and the ligand-binding groove. Current sensor technologies utilize biosensors that are based on the carbohydrate moieties that are involved in pathogen adhesion to host cells. Nanoparticles have been extensively used as carriers for pathogen detection. Gold nanoparticles (Au NPs) of 200 nm size were functionalized with two distinct glycoconjugates mannose (Mn–Au NPs) and Neu α (α 2-3)-Gal-(β 1-4)Glc–Paa (Sg–Au NPs) in order to investigate primary and fine sugar specificity of uropathogenic *E. coli* ORN178 and enterotoxigenic *E. coli* 13762, respectively. The UV-Vis measurement of pristine, 16-mercaptohexadecanoic acid (MHDA)/2-(2-aminoethoxy) ethanol (AEE)/sugar functionalized Au NPs showed a surface plasmon resonance band for Au. Dynamic light scattering analysis showed that the mean averages of the MHDA/AEE/Mn–Au NP samples increased due to aggregation. The negative zeta potentials of the samples were indicative of aggregation. Fine sugar specificity was observed when Neu α (α 2-3)-Gal-(β 1-4)Glc–Paa functionalized Au

NPs (Sg–Au NPs) specifically showed binding with *E. coli* 13762 but not with *E. coli* ORN178. This specificity of *E. coli* strains to identify and bind to characteristic sugar moieties can be used in the development of biodiagnostic tools with Au NPs as carriers for diagnosis/treatment of human and veterinary diseases. In regards to the growing antibiotic resistance of microorganisms, gold nanoparticles can also be functionalized specifically to reverse adhesion of *E. coli* to host tissue and can be detected by their optical properties.

Keywords Gold nanoparticles · *E. coli* · Lectins · Fimbrial adhesion · Nanotechnology · Binding · Aggregation · Surface plasmon resonance · Zeta potential · Pathogen detection

Introduction

Tools for the study of bimolecular interactions have been developed based on the surface plasmon resonance of functionalized nanoparticles. Surface functionalization has proved to impart biofunctionality and this property has been exploited in developing different kinds of biosensors [1].

Although the application of colloidal metal nanoparticles in biology is not new, the optical observation of single metal particle labels and aggregated nanoparticles is of interest as a component of ultrasensitive detection systems. The surface plasmon resonance (SPR) is indicative of the light scattering by nanometer-sized colloidal metal particles. The function of the size, shape, particle properties can be inferred from the color of the light scattered. Colloidal gold nanoparticles (Au NPs) are brilliant red in color. Hence, biosensors, identification and detection systems of biomolecules can be developed based on the shift in SPR [2]. Haynes et al. [3] developed a biosensor that works by measuring a shift in the plasmon resonance peak induced by the local

P. Vedantam · T.-R. J. Tzeng (✉) · A. K. Brown · K. Staley
Department of Biological Sciences, Clemson University,
Clemson, SC 29634, USA
e-mail: tzuenrt@clemson.edu

R. Podila
Department of Physics and Astronomy, Clemson University,
Clemson, SC 29634, USA

A. Rao
Medical University of South Carolina,
Charleston, SC, USA

dielectric environment. Haes et al. [4] measured a shift in the PR peak caused by a change in the local dielectric environment in silver nanoparticle arrays that could function as sensitive and selective nanoscale affinity biosensors.

Colloidal Au NPs tend to settled down after a few hours. By adjusting the distance between discrete nanoparticles or layers of nanoparticles, the SPR can be controlled [5]. The peak of extinction will reduce, as the aggregate size increases shifting and broadenign the red plasmon band. Storhoff et al. [6] have reported that extinction spectra for DNA-linked gold nanoparticle aggregates composed of equal number of particles but with smaller separations between particles and have red shift in the plasmon peak without causing significant loss in peak extinction. The optical response of a particular nanoparticle depends on its size and shape that defines the intrinsic modes as well as the dielectric environment that typically define the energy shifts. Taking advantage of the optical and electronic properties, Au NPs have been used in bioassays such as detection of DNA hybridization, probing binding to citrate-coated Au NPs [7, 8].

Another application of biodetection is the use of nanoparticles extensively in pathogen detection [9, 10]. Pathogens bind to eukaryotic cell membranes by crucial interactions with biomolecules on the surface of the cells. There is a lot of evidence that the complex oligosaccharides in the glycocalyx are key players in controlling the normal and pathological processes [11, 12] in mammalian cells. Glyconanoparticles could hence mimic a cellular model with carbohydrate presented on the cell surface, which can be used as excellent tools in biomedicine and glycobiology studies. Firstly, their size is in range to many common biomolecules; secondly, carbohydrate-modified nanoparticles can mimic biomolecules; thirdly, they provide glycocalyx-like surface properties and lastly, they have unique physical properties due to the quantum size effect [13, 14].

Many groups have functionalized Au NPs with mono-, di-, tri-, or oligo-saccharides [15–19] with applications in biosensing, drug delivery, vaccine development, and in vivo cell imaging. For instance, our previous research has demonstrated that, galactosylated polymeric polystyrene nanoparticles have shown significant aggregation when incubated with *Escherichia coli* [20]. UV–vis extinction properties of DNA-linked nanoparticle aggregates have been determined [21] and it is seen that depending on the particle volume fraction the aggregate size increases, the surface plasmon absorption peak shifts to longer wavelengths throughout the UV–vis range. This suggests that the denser and larger the aggregates, broader the plasmon feature. The shift in the SPR can be manipulated in designing biosensors that involve pathogen detection systems.

By the use of glyan-coated Au NPs, the attachment/detachment mechanism of potential pathogens to Au NPs

could be assessed and the optical properties displayed by the colloidal Au NPs can be measured. We investigated the role of sugar functionalized 200 nm (Au NPs) in determining primary and fine sugar specificity in *E. coli* ORN178 and *E. coli* 13762. *E. coli* ORN178, which is a wild-type that causes urinary tract infection. It has type 1 fimbrial protein that confers the unique quality of binding to D-mannose only [22]. We used *E. coli* ORN208 as a negative control. It has abnormal type 1 pili that fail to bind to D-mannose [23]. The other one is *E. coli* American Type Culture Collection (ATCC) 13762 which causes enterotoxigenic diarrhea. *E. coli* 13762 is known as a K99+ strain that expresses K99 antigen that enters the humans as a foodborne pathogen via meat products especially in contaminated porcine meat. It has S type fimbrial proteins and binds specifically to Neu α (α 2-3)-Gal-(β 1-4)Glc [24].

Material and Methods

The strains *E. coli* ORN178 and ORN208 were kindly provided by Dr. Chu-Cheng Lin, Department of Zoology, National Taiwan Normal University, Taiwan. *E. coli* 13762 and yeast strain *Saccharomyces cerevisiae* were obtained from the ATCC (Manassas, VA, USA). *E. coli* ORN178, ORN208 and 13762 were transformed with plasmid pGREEN by electroporation [25]. Green fluorescent protein (GFP)-expressing bacterial cells of the three select strains were harvested from a trypticase soy agar medium supplemented with ampicillin (50 μ g/ml).

Colloidal Au NPs of 200 nm size of 7×10^8 particles/ml concentration were purchased from, Ted Pella Inc. (USA). The Neu α (α 2-3)-Gal-(β 1-4)Glc–Paa (Sg) was procured from Glyco Tech Corporation (USA) and D-mannan (Mn) was purchased from VWR (USA). The sugars were dissolved in 0.3 M sodium phosphate buffer. Absolute ethanol, 2-(2-aminoethoxy)ethanol (AEE) and *N*-hydroxy-2,5-pyrrolidinedione (NHS), 16-mercaptohexadecanoic acid (16-MHDA), epichlorohydrin, 2-methoxyethyl ether (diglyme), *N*-3-(dimethylaminopropyl)-*N'*-ethyl-carbodiimide (EDC) were obtained from VWR (USA).

Sodium phosphate monobasic buffer solution (10 mM) concentration at pH 7 was used. PBS of pH 7.4 in deionized water was used. All buffers were prepared in deionized water (>18 M Ω /cm). Glassware was washed with “piranha solution” (3:7, 30% H₂O₂/H₂SO₄). Degassed ethanol was used to prepare 0.50 mM 16-MHDA.

Preparation of Functionalized Au NPs The surface modification of the gold colloids was carried out by a modified multistep procedure [26]. Tween 20 was not used for physisorption as the nanoparticles' surfaces were plain with no charges. Briefly, the Au NPs were degassed with Argon

gas. Equal volumes (500 μl) of 200 nm Au NP dispersions and 0.50 mM 16-MHDA was then added and the final mixture was allowed to stand for 3 h for the chemisorption of 16-MHDA to gold colloids. Excess 16-MHDA was removed by centrifuging the mixture three times for 5 min at $1,699\times g$; the supernatants were discarded after each cycle and resuspended in phosphate buffer. 16-MHDA-modified gold colloids that remained in the centrifugate were then reacted with a mixture of freshly prepared 50 mM NHS and 200 mM EDC solution for 5 min. The resulting nanoparticle dispersion was centrifuged at 5 min, $1,699\times g$. The supernatant was discarded, the remaining NHS ester-alkane thiol-modified Au NPs were reacted with a freshly prepared solution of AEE (2%, v/v) for 10 min. Excess AEE was removed by centrifugation for 5 min at $1,699\times g$ at least three times. The pellet that contained AEE-modified Au NPs was centrifuged (5 min, $1,699\times g$). The hydroxyl groups on the AEE-modified Au NPs were activated with 0.6 M epichlorohydrin solution in a 1:1 mixture of 0.4 M NaOH and diglyme for 4 h at room temperature. The nanoparticle dispersion was then centrifuged for 10 min at $1,699\times g$ and resuspended in diglyme and centrifuged again to remove the excess epichlorohydrin. The centrifugate, containing AEE-modified Au NPs now with active epoxide groups, were incubated in two glycan solutions namely, Sg and Mn solutions (0.1 M NaOH) for 20 h. Finally, Sg- and Mn-modified Au NPs were centrifuged for 5 min at $1,699\times g$ and resuspended in 0.1 M NaOH and centrifuged four more times to remove the excess sugar. The different sugar modified Au NPs: Mn–Au NPs and Sg–Au NPs were stored in Eppendorf tubes wrapped with aluminum foil in order to avoid aggregation induced by light.

The UV–vis measurement for four selected functionalized Au NP samples: pristine Au NP, MHDA–Au NP, AEE–Au NP, and *E. coli* ORN178 bound to Mn–Au NPs was carried out using a LAMBDA 950 UV/Vis/NIR Spectrophotometer (Perkin-Elmer, USA). Hydrodynamic diameter and size distributions for the four Au NP samples in aqueous

solutions were determined by dynamic light scattering (DLS). The DLS instrumentation consisted of Malvern Zetasizer Nano ZS (Worcestershire, UK) system, ZEN3600 model. Measurements of diameter and ζ potential were made at $25\pm 1^\circ\text{C}$. The ζ average diameter reported herein was obtained as the average of three measurements performed on each sample. The morphology of the samples was imaged using a Hitachi S3400 scanning electron microscopy (SEM) model. A drop of the samples was put on poly-L-lysine-coated Si substrates, was air dried for 2 h and observed under SEM.

Results

Transformation of *E. coli* Strains

The *E. coli* ORN178, ORN208, and 13762 were successfully transformed (Fig. 1). The transformants fluoresced when viewed under the fluorescent scope (Zeiss LSM-510) under the GFP filter. *E. coli* ORN178 (Fig. 1a) and ORN208 (Fig. 1b) appeared to be considerably longer rods when compared to the short rods of *E. coli* 13762 (Fig. 1c).

Yeast Agglutination Assay

The mannose-binding characteristics of the transformants were verified using a yeast agglutination assay [27] to document that the transformation had not altered the previously determined mannose-binding characteristics of *E. coli* ORN178 and ORN208. The binding specificity of *E. coli* 13762 to mannose was also determined. Figure 2a shows the transformant *E. coli* ORN178, not the ORN208 (Fig. 2b), mediated the agglutination of yeast cells. Both strains were found to retain the same characteristics as their parent strains regarding their mannose-binding activities. *E. coli* 13762 (Fig. 2c) did not show any visible binding to yeast cells both in the fluorescent and brightfield images indicating that they lack type 1 binding fimbria.

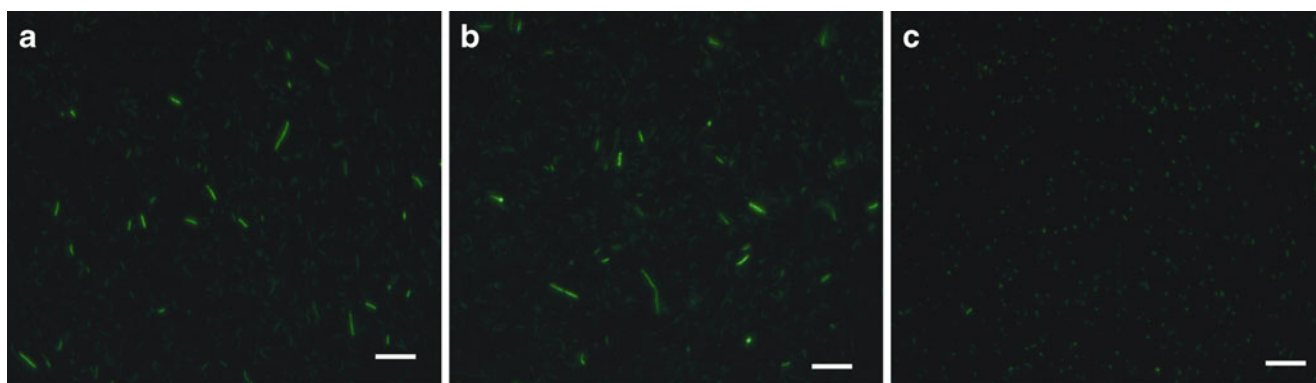


Fig. 1 Fluorescent images of **a** *E. coli* ORN178, **b** *E. coli* ORN208, and **c** *E. coli* 13762 as seen at $400\times$ magnification. Scale bar 10 μm

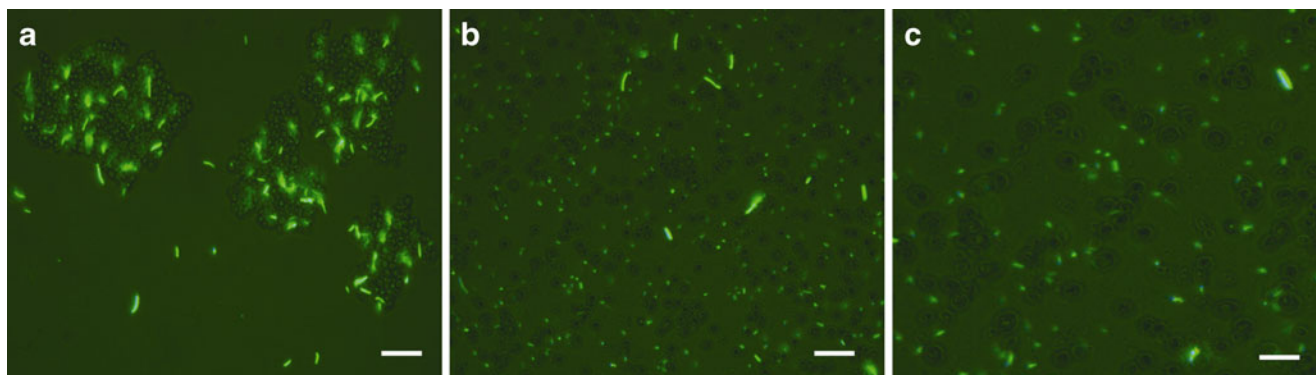


Fig. 2 Yeast agglutination assay. **a** *E. coli* ORN178 binds to yeast cells and bring about clumping (400 \times), **b** no binding is seen in case of *E. coli* ORN208 (400 \times), and **c** shows no binding of *E. coli* 13762 with yeast cells. Scale bar 10 μ m

UV–Vis Analysis

We report here the studies of UV–visible absorption spectroscopy, DLS and SEM on pristine, MHDA, AEE–Au NPs and binding of *E. coli* ORN178 to Mn functionalized Au NPs. The SPR absorbance was found to be similar in the case of Sg–Au NPs bound to *E. coli* 13762; hence, we chose to present the absorbance of Mn–Au NPs. The plasmon band observed for the pristine Au NPs was at 570 nm which is characteristic of 200 nm Au NPs (Fig. 3). The initial

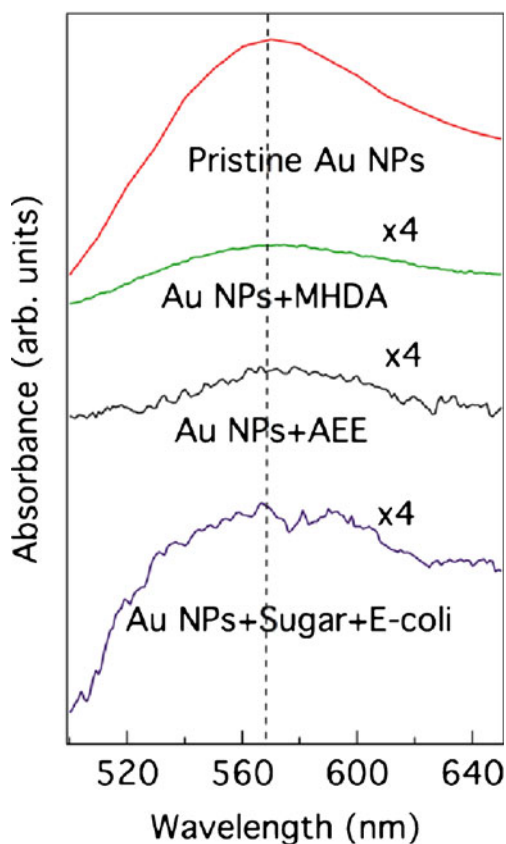


Fig. 3 UV–vis absorbance of plain, 16-MHDA modified Au NP and Mn–Au NPs bound to *E. coli* ORN178

characterization of MHDA and AEE–Au NPs also showed absorption maximum of the surface plasmon band at 570 nm indicating the presence of functionalized Au NPs in the functionalized samples. The Mn–Au NPs when bound to *E. coli* ORN178 also displayed a SPR band of 570 nm. It is clearly seen that Au NPs keep their nanoform even after chemical modifications. Although MHDA–Au NPs and AEE–Au NPs do aggregate as seen in Fig. 4b, c, their size remains the same according to the DLS data obtained (Table 1). Figure 4d shows the binding of *E. coli* ORN178 to the Mn–Au NPs. The pristine Au NPs as seen in the SEM image (Fig. 4a) remain suspended, but the other samples do tend to aggregate to a little extent. The diameters of the samples measured in dispersion are listed in Table 1. The DLS data shows that that the mean diameter of pristine Au NPs is 213.5 nm. The diameter range of the pristine Au NPs is

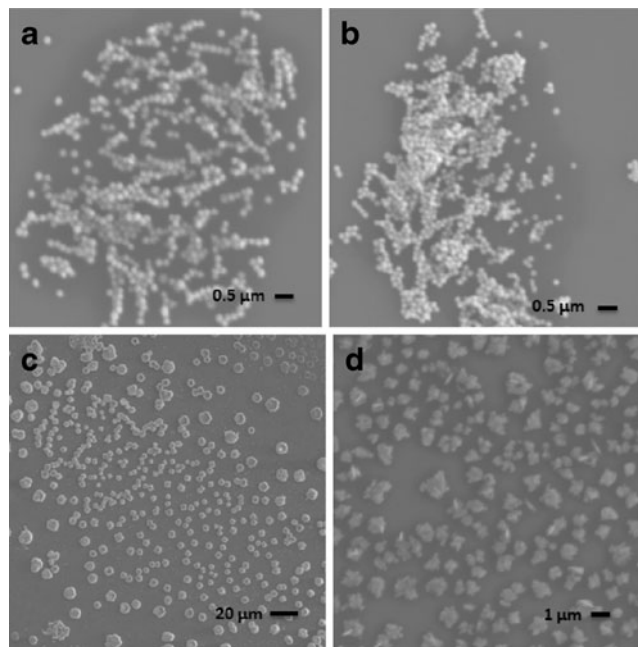


Fig. 4 SEM images of **a** pristine Au NPs, **b** MHDA Au NPs, **c** AEE–Au NPs, and **d** aggregate of Mn–Au NPs and *E. coli* ORN178

Table 1 DLS mean diameters and zeta potentials of functionalized Au NPs

Sample	z (mV)	Mean size (nm)
Pristine Au NPs	-49.3	213.5
MHDA–Au NPs	-36.6	226.4
AEE–Au NPs	-14.0	462.7
Mn–Au NPs	-9.82	5,076

slightly larger than the quoted by the manufacturer (200 nm). This is not unexpected, as the DLS system is measuring the hydrodynamic size of the hydrated particles.

The mean size of the MHDA–Au NP, AEE–Au NP, and *E. coli* ORN178 bound to Mn–Au NPs increase due to aggregation. All the four samples indicated a negative charge as determined by ζ potential measurements. The ζ potential of the four samples ranged from -49.3 to -9.82 mV as the size of the sample increases. Mean ζ potential value of pristine Au NP colloids has been reported to be -42.5 [28], the values listed in Table 1 are consistent. As the Au NPs get functionalized they tend to aggregate and hence, could tend to be more unstable as a result of aggregation. This could cause the drop in ζ potential -49.3 mV of pristine Au NPs to -9.82 mV of the Mn–Au NPs bound to *E. coli* ORN178.

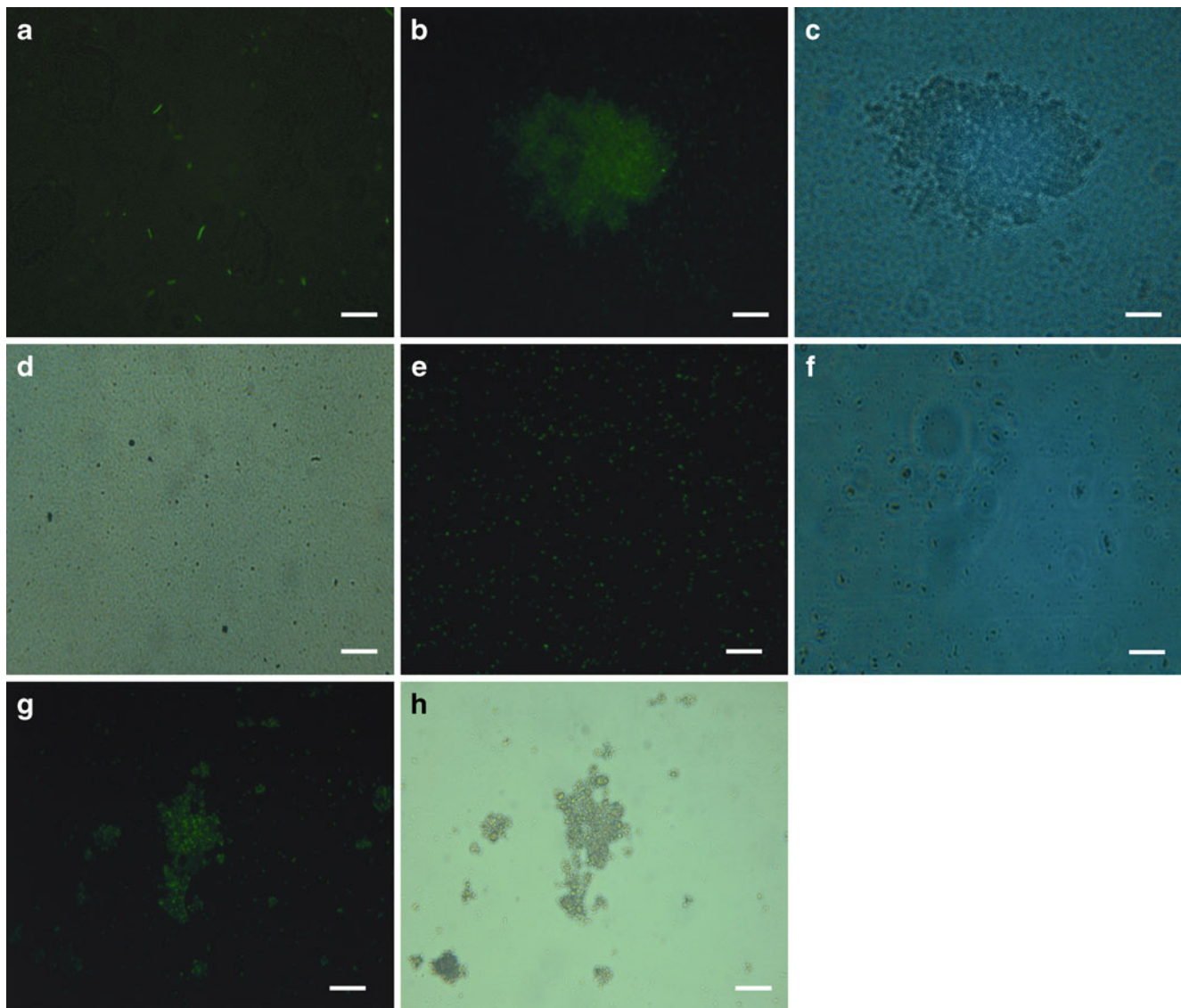


Fig. 5 Bacterial agglutination by sugar functionalized AuNPs. **a** Control: plain AuNPs with *E. coli* ORN178, **b** fluorescent image of Mn–Au NPs and *E. coli* ORN178, **c** brightfield image of Mn–Au NPs and *E. coli* ORN178, **d** negative control: bright filed image of *E. coli* ORN208 and Mn–Au NPs, **e** fluorescent image of *E. coli* 13762 and

Mn–Au NPs, **f** bright field image of *E. coli* 13762 and plain Au NPs, **g** fluorescent image of *E. coli* 13762 and Sg–Au NPs and **h** brightfield image of *E. coli* 13762 and Sg–Au NPs. All images are in 400 \times . Scale bar 10 μ m

Binding of *E. coli* to Au NPs

Binding specificities were examined as depicted in Fig. 5. After incubation of Mn–Au NPs with the *E. coli* ORN178 cells formed bacterial clumps, which emitted a bright fluorescence signal. These bacterial clumps consisted of hundreds of aggregated bacterial cells. The Mn–Au NPs were found to aggregate in the presence of *E. coli* ORN178 only. Binding was in accordance to the yeast agglutination assay results showing that *E. coli* ORN178 has specific binding to mannan (Fig. 5b, c). *E. coli* 13762 did not show any binding to Mn–Au NPs, but consistently binds specifically to Sg–Au NPs (Fig. 5e, f). Bacterial clumps were formed by agglutination of Sg–Au NPs and *E. coli* 13762 (Fig. 5g, h). This proves that the two different *E. coli* have different binding specificities. The *E. coli* ORN178 did not show binding to Sg–Au NPs. Specific binding of Mn–Au NPs to *E. coli* ORN178 and binding of Sg–Au NPs to *E. coli* 13762 have been demonstrated. This phenomenon is not a result of adsorption because no binding has been observed with bare Au NPs lacking the Mannan or the Sg moieties (Fig. 5a). *E. coli* ORN208 was used as a negative control in our experiments. It was not surprising that the abnormal type 1 pili expressing ORN208 clearly exhibited no binding to Au NPs, Mn–Au NPs, or Sg–Au NPs.

An example of non-attachment of *E. coli* ORN208 with Mn–Au NPs (Fig. 5d) is presented to show no binding. Samples at various stages of functionalization were kept aside to test binding of all the three bacterial strains. The intention was to see if any of the 16-MHDA/NHS/AEE/ECH-modified Au NPs could mediate aggregation by the means of surface absorption. Except for the sugar-modified Au NPs, no binding occurred during the course of the multistep reaction.

Discussion

The optical spectrum of colloidal gold suspensions is dominated by SPR band, which is due to the collective dipole oscillation in the conduction band of gold. The position, intensity, and the shape of the plasmon resonance band are influenced by many factors such as particle size and shape, dispersity, and degree of aggregation [28]. Dielectric constant and other stabilizing agents play an important role in conduction of Au band [2]. The longitudinal plasmon resonance band has also been found indicative of Au NPs coming in close proximity during aggregation. Diegoli et al. [28] have also shown that there is a distinctive region in the plots of ζ potential versus particle concentration, in which the ζ potential value is independent of nanoparticle concentration. It is referred to as the “stable region” of the plot. The results showed sample

stability was indicated by their large negative ζ potential values, with the average mean ranging from -43 to -56 mV. Moreover, DLS and SEM results in this study have corroborated the results obtained by UV–visible spectroscopy. Thus, by exploiting the sensitivity of the optical parameters of particles, Au NPs can be used as a novel tool for pathogen detection which in this case is based on microbiological aspect of the *E. coli* strains binding to different sugars is simply based on their structural characteristics. The most important life style of *E. coli* is its mechanism of attachment to host tissue. The myriad adhesins discovered in *E. coli* to demonstrate the fact that it is an important determinant in establishment of bacterial attachment followed by colonization and infection. Pathogenic *E. coli* expresses many different kinds of adhesins which can be grouped according to their affinity to specific receptor structures. The functional organization of fimbrial lectin is different with respect to the position of the receptor binding sites. Primary sugar specificity or the fine sugar specificity by and large defines the specificity of the fimbrial lectin. The former refers to a simple carbohydrate structure, for example a monosaccharide that can inhibit the lectin mediated adhesion; whereas the latter refers to differences in binding to different oligosaccharides in lectins demonstrating the same primary sugar specificity [29]. Many enterobacteria express D-mannose lectins, which conform to the primary sugar specificity for type 1 fimbriae. Enterobacterial fimbrial adhesins that have been characterized according to their sugar specificities [29]. They are α -D-mannosides (type 1 fimbrial adhesin), α -D-Gal-(1–4)- β -D-Gal (P fimbrial adhesin), and NeuAc α 2,3-galactose (S fimbrial adhesin) [30, 31].

The type 1 fimbria of *E. coli* ORN178 consists of mannose binding FimH lectin that aids in binding to glycoproteins that are a part of the adhesive domain on host cells. The globoside-binding P fimbria of uropathogenic *E. coli* has shown to bind to the urolapkins on the surface of urothelial cells of the human bladder [32, 33]. Not only the type 1 fimbrial proteins have demonstrated a vital role in colonization of *E. coli* on host intestinal surfaces, they also play a role in causing urinary tract infections [34]. The enterotoxigenic (ETEC) *E. coli* (K99) causes diarrhea in animals such as pigs, calves, and lambs [35]. A ganglioside glycolipid in FanC is involved in fimbrial adhesion, which consists of tetrasaccharide GalNAc β -3Gal α 1-4Gal β 1-4Glc in the binding pocket of K99. This ceramide when involved in lectin-binding pocket interaction brings about considerable conformational change in the binding protein that causes adhesion to host cells [36]. Based on these factors, two different types of *E. coli* strains were selected in order to study their binding specificity and from Fig. 5 we can clearly concur that the primary and fine sugar specificities do play an important role in pathogenesis.

The yeast agglutination assay clearly indicated primary specificity by type 1 mediated binding of *E. coli* ORN178 to mannan residues on the surface of yeast cells. On the contrary, fine sugar specificity brought about no agglutination in *E. coli* 13762 (aka *E. coli* K99) with yeast cells as it exhibits type S fimbrial adhesins. It recognizes only a specific oligosaccharide sequence, i.e., NeuAc(α 2-3)Gal(β 1-4), which is not a part of yeast cell surface receptors. Due to the presence of abnormal pili, *E. coli* ORN208 failed to bind to yeast cells. A detailed study where mannan Au NPs have been used to observe the specific binding to FimH adhesin of bacterial type 1 pili by TEM has been demonstrated [30]. This establishes that aggregation of *E. coli* ORN178 was induced specifically by mannan recognition on the surface of the yeast cells.

Conclusion

The UV–vis measurements indicate the presence of Au SPR band confirming the nanoform of the particles despite functionalizing them. The mean sizes of the four select samples increased due to aggregation. The ζ potential dropped as the particles changed from a suspended to an aggregated state. We also found that mannan functionalized Au NPs (Mn–Au NPs) specifically bind with *E. coli* ORN178 only but not with *E. coli* 13762. Fine sugar specificity was observed when NeuAc(α 2-3)-Gal-(β 1-4)Glc–Paa functionalized Au NPs (Sg–Au NPs) specifically showed binding with *E. coli* 13762 but not with *E. coli* ORN178. These results indicate that the binding induced by sugar-modified Au NPs is specific to the characteristic sugar that bacteria recognize on binding sites located around the cell surface and that such glyconanoparticles have the potential use in the identification of pathogens and also competitively prevent the binding of microorganisms to the eukaryotic cell surface receptors.

Biofunctionalized nanoparticles can serve as excellent carrier systems. With multiple receptors immobilized on carrier surface, each particle could interact with multiple bacteria resulting in the formation of aggregates. Merging of multiple aggregates mediated by these carrier particles could further prevent the bacteria from attaching to the host cells, especially in the urinary and the intestinal tracts owing to the high peristaltic pressures. The in vivo effects of the surface chemistry of the functionalized nanoparticles and their behavior in the UTI/intestinal tract warrant further investigation.

It is seen that UTI causing *E. coli* ORN178 evidently binds only to Mn–Au NPs and not to Sn–Au NPs. And ETEC 13762 exhibited specificity in binding to only Sn–Au NPs and not to mannan. This indicates that there is high specificity in adhesin mediated binding exhibited by different microorganisms. From the above discussion, it is clear that type 1 specificity is exhibited by many microorganisms

that can easily bind to D-mannose and mediate generic adhesion, whereas certain microorganisms also recognize specific carbohydrate sequence which defines their fine sugar specificity. In the latter case, there is adhesin-specific adhesion that is not generic in nature. This means that binding of microorganisms can be altered with the use of carbohydrate functionalized nanoparticles to competitively bind to the cell surface receptors and block the adhesion of pathogens.

Theoretically, it can be envisioned that in such a scenario, binding can be reversed by aggregation of large amounts of functionalized Au NPs clumping together and detaching the bacteria from the cell surface. Such nanoparticles could lead to the development of diagnostic tools that not only identify generic binding but also, can detect presence of specific species in a given genus. With the fast emerging antibiotic/drug-resistant strains, nanoparticles may be employed to reduce the microbial load in diagnosis/treatment of medical diseases, contamination of food products, treatment of meat and poultry products, as carriers to deliver a particular drug for a localized effect, bioimaging of tissues, and lastly as models for repairing cellular functions and alter pathogenesis. Our results thereby indicate that blockage of bacterium–host interaction by specific sugar-modified Au NPs can be an effective method for removal of bacteria from hosts and detection of specific optical properties of the nanoparticles used can further assess the extent of binding.

Acknowledgments We thank Dr. Pu-Chun Ke, Associate professor (Physics), Clemson University, for the use of UV–vis instrument. We are highly grateful to Dr. Bevan Elliot, associate research chemist at the University of Dayton Research Institute for helpful discussions and insights on Au NPs. We would also like to acknowledge Dr. Sai Sathish, Sri Sathya Sai Institute of Higher Learning, and Dr Ramakrishna Podila, Research Associate in the Department of Physics and Astronomy, Clemson University for their valuable technical assistance.

References

1. Wijaya E et al (2011) Surface plasmon resonance-based biosensors: from the development of different SPR structures to novel surface functionalization strategies. *Curr Opin Solid State Mater Sci* 15(5):208–224
2. David AS (2003) Plasmon resonant particles for biological detection. *Curr Opin Biotechnol* 14(1):13–22
3. Haynes CL, Van Duyne RP (2001) Nanosphere lithography: a versatile nanofabrication tool for studies of size-dependent nanoparticle optics. *J Phys Chem B* 105(24):5599–5611
4. Haes AJ, Van Duyne RP (2002) A nanoscale optical biosensor: sensitivity and selectivity of an approach based on the localized surface plasmon resonance spectroscopy of triangular silver nanoparticles. *J Am Chem Soc* 124(35):10596–10604
5. Schmitt J et al (1997) Metal nanoparticle/polymer superlattice films: fabrication and control of layer structure. *Adv Mater* 9(1):61–65
6. Storhoff JJ et al (2000) What controls the optical properties of DNA-linked gold nanoparticle assemblies? *J Am Chem Soc* 122(19):4640–4650

7. Aizpurua J et al (2003) Optical properties of gold nanorings. *Phys Rev Lett* 90(5):057401
8. Brewer SH et al (2005) Probing BSA binding to citrate-coated gold nanoparticles and surfaces. *Langmuir* 21(20):9303–9307
9. Rosi NL, Mirkin CA (2005) Nanostructures in biodiagnostics. *Chem Rev* 105(4):1547–1562
10. Jain KK (2005) Nanotechnology in clinical laboratory diagnostics. *Clin Chim Acta* 358(1–2):37–54
11. Varki A (1993) Biological roles of oligosaccharides: all of the theories are correct. *Glycobiology* 3:1297–1340
12. Dwek RA (1996) Glycobiology: toward understanding the function of sugars. *Chem Rev* 96(2):683–720
13. Murray CB, Kagan CR, Bawendi MG (2000) Synthesis and characterization of monodisperse nanocrystals and close-packed nanocrystal assemblies. *Annu Rev Mater Sci* 30(1):545–610
14. López-Cartes C et al (2005) Gold nanoparticles with different capping systems: an electronic and structural XAS analysis. *J Phys Chem B* 109(18):8761–8766
15. Zhang J, Geddes CD, Lakowicz JR (2004) Complexation of polysaccharide and monosaccharide with thiolate boronic acid capped on silver nanoparticle. *Anal Biochem* 332(2):253–260
16. Svarovsky SA, Szekeley Z, Barchi JJ (2005) Synthesis of gold nanoparticles bearing the Thomsen–Friedenreich disaccharide: a new multivalent presentation of an important tumor antigen. *Tetrahedron-Asymmetry* 16(2):587–598
17. Lin CC et al (2003) Quantitative analysis of multivalent interactions of carbohydrate-encapsulated gold nanoparticles with concanavalin A. *Chem Commun (Camb)* 23:2920–1
18. Takae S et al (2005) Ligand density effect on biorecognition by PEGylated gold nanoparticles: regulated interaction of RCA120 lectin with lactose installed to the distal end of tethered PEG strands on gold surface. *Biomacromolecules* 6(2):818–824
19. Aslan K, Lakowicz JR, Geddes CD (2004) Nanogold-plasmon-resonance-based glucose sensing. *Anal Biochem* 330(1):145–155
20. Qu L et al (2005) Galactosylated polymeric nanoparticles: synthesis and adhesion interactions with *Escherichia coli*. *J Biomed Nanotechnol* 1:61–67
21. Lazarides AA, Schatz GC (1999) DNA-linked metal nanosphere materials: structural basis for the optical properties. *J Phys Chem B* 104(3):460–467
22. Harris SL et al (2001) Characterization of *Escherichia coli* type 1 pilus mutants with altered binding specificities. *J Bacteriol* 183(13):4099–4102
23. Krogfelt KA, Bergmans H, Klemm P (1990) Direct evidence that the FimH protein is the mannose-specific adhesin of *Escherichia coli* type 1 fimbriae. *Infect Immun* 58(6):1995–1998
24. Sharon N (2006) Carbohydrates as future anti-adhesion drugs for infectious diseases. *Biochim Biophys Acta (BBA)–General Subjects* 1760(4):527–537
25. Sambrook J, Russell DW (eds) (2001) *Molecular cloning: a laboratory manual*, 3rd edn. Cold Spring Harbor Laboratory Press, Cold Spring Harbor
26. Aslan K, Lakowicz JR, Geddes CD (2004) Tunable plasmonic glucose sensing based on the dissociation of Con A-aggregated dextran-coated gold colloids. *Anal Chim Acta* 517(1–2):139–144
27. Ofek I, Mirelman D, Sharon N (1977) Adherence of *Escherichia coli* to human mucosal cells mediated by mannose receptors. *Nature* 265(5595):623–625
28. Diegoli S et al (2008) Interaction between manufactured gold nanoparticles and naturally occurring organic macromolecules. *Sci Total Environ* 402(1):51–61
29. Sharon N, Ofek I (2000) Safe as mother’s milk: carbohydrates as future anti-adhesion drugs for bacterial diseases. *Glycoconj J* 17(7):659–664
30. Lin CC et al (2002) Selective binding of mannose-encapsulated gold nanoparticles to type 1 pili in *Escherichia coli*. *J Am Chem Soc* 124(14):3508–3509
31. Sokurenko EV et al (1997) Diversity of the *Escherichia coli* type 1 fimbrial lectin. Differential binding to mannosides and uroepithelial cells. *J Biol Chem* 272(28):17880–17886
32. Westerlund-Wikström B, Korhonen TK (2005) Molecular structure of adhesin domains in *Escherichia coli* fimbriae. *Int J Med Microbiol* 295(6–7):479–486
33. Wu XR, Sun TT, Medina JJ (1996) In vitro binding of type 1-fimbriated *Escherichia coli* to uroplakins Ia and Ib: relation to urinary tract infections. *Proc Natl Acad Sci U S A* 93(18):9630–9635
34. Hung C-S et al (2002) Structural basis of tropism of *Escherichia coli* to the bladder during urinary tract infection. *Mol Microbiol* 44(4):903–915
35. Simons BL et al (1990) Structure, localization and function of FanF, a minor component of K99 fibrillae of enterotoxigenic *Escherichia coli*. *Mol Microbiol* 4(12):2041–2050
36. Simons LH et al (1991) Localization and function of FanH and FanG, minor components of K99 fimbriae of enterotoxigenic *Escherichia coli*. *Microb Pathog* 11(5):325–336